Clays and Clay Minerals, Vol. 50, No. 2, 157–173, 2002.

TRANSMISSION ELECTRON MICROSCOPY STUDY OF SMECTITE ILLITIZATION DURING HYDROTHERMAL ALTERATION OF A RHYOLITIC HYALOCLASTITE FROM PONZA, ITALY

BLANCA BAULUZ[1], DONALD R. PEACOR[2] AND ROBERT F. YLAGAN[3]

[1] Departamento de Ciencias de la Tierra, Cristalografía y Mineralogía, Universidad de Zaragoza, 50.009 Zaragoza, Spain
[2] Department of Geological Sciences, The University of Michigan, Ann Arbor, Michigan 48109-1063, USA
[3] ExxonMobil Upstream Research Company, P.O. Box 2189, Houston, Texas 77252-2189, USA

Abstract—Dioctahedral phyllosilicates from an altered rhyolitic hyaloclastite located at Ponza Island, Italy, were studied by scanning electron microscopy (SEM) and transmission electron microscopy (TEM). The samples are from a sequence previously characterized by X-ray diffraction (XRD) methods, indicating that a complete range of illitization accompanies alteration. Backscattered electron (BSE) images, obtained from ion-milled samples, show that samples partly retain the original textures since clay minerals pseudomorph lapilli fragments and preserve vesicular texture. The lowest-grade sample studied contains obsidian clasts partially replaced by smectite. As the alteration grade increases, illitization proceeds with formation of interstratified illite-smectite (I-S), zeolites, illitic phases, feldspars and quartz. The most altered sample contains illite, mica and quartz. Lattice-fringe images show that following the formation of smectite, illitization takes place through the formation of (R=1) I-S, highly illitic I-S and illite with mica; (R=1) I-S is the only ordered interstratified I-S. The BSE and TEM images of Ponza samples show irregular cavities filled with euhedral dioctahedral clay minerals and the zeolite mordenite, providing direct evidence for neocrystallization from a fluid. Chemical compositions by analytical electron microscopy (AEM) support the sequence described. Selected area electron diffraction (SAED) patterns indicate the predominance of $1M_d$ polytypism both in I-S and illitic phases, and the coexistence in the more altered samples of $1M_d$ illite and a 2-layer mica polytype (probably $2M_1$), without the intermediate $1M$ polytype generally assumed to exist in prograde sequences. Previous XRD studies indicated progressive change from *cis*-vacant, turbostratically stacked smectite, to interstratified *cis*- and *trans*-vacant, $1M_d$ I-S, to *trans*-vacant, $1M$ illite, and then to $2M_1$ illite in Ponza Island samples. We observed a clear correlation between the chemical compositions as determined by AEM and the proportion of *cis*-vacant determined by XRD, suggesting that the octahedral cation distributions change in the studied samples with increasing degree of illitization.

Key Words—Hydrothermal alteration, Illite-Smectite (I-S), Illitization, Polytypes, Scanning Electron Microscopy, Transmission Electron Microscopy.

INTRODUCTION

The transition from smectite to illite has been widely documented by XRD studies. From the time of the pioneering study of Hower *et al.* (1976), there has been general agreement that this process involves interstratified (I-S) intermediates, with the proportion of illite in mixed-layer I-S increasing as a function of increasing temperature, time and burial depth of basin sediments. Most studies of illitization use modeled XRD patterns of I-S to document changes in ordering of high- and low-charge layers using the Reichweite (R) notation, where R represents the number of layers affected by the presence of a given layer (Jadgozinski, 1949). Numerous studies of smectite illitization reported that smectitic I-S exhibits R=0 ordering, illitic I-S has R=1 ordering and highly illitic I-S has R=3 ordering (Hower *et al.*, 1976; Altaner *et al.*, 1984; Horton, 1985; Brusewitz, 1986). Ordering of individual interlayers within I-S packets can be directly identified in TEM images. Recently, Bauluz *et al.* (2000) suggested a nomenclature for expressing I-S ordering as seen in TEM images. They suggested use of the symbol I*n*, where *n* is the number of illite-like layers associated with a given smectite-like layer; *i.e.* two 2:1 layers of IS-type are denoted as an I1 unit, ISI as an I2 unit, *etc.* An ideal sample for which R = 1, with 50% illite-like layers, is identical to a sequence of I1 units, for example, but a sequence for which R = 1, > 50% I would consist dominantly of I1 units, but also have units with $n>1$.

Several TEM studies indicated that (R=1) I-S ($\geqslant$50% illite) is relatively abundant, whereas other ordered I-S sequences with R>1 are rarely observed (Ahn and Peacor, 1989; Veblen *et al.*, 1990; Jiang *et al.*, 1990; Dong and Peacor, 1996; Dong *et al.*, 1997), *i.e.* I1 units were abundant in the studied samples but I*n*, with $n>1$ were scarce. Dong *et al.* (1997) studied smectitic and illitic clays from several occurrences and lithologies (shales from the Gulf Coast, Nankai Trough, Japan, the Michigan Basin, the Welsh sedimentary basin, and hydrothermally altered bentonite from Zempleni, Hungary). All samples

* E-mail address of corresponding author:
bauluz@posta.unizar.es

showed different proportions of discrete layer sequences of smectite, (R=1) I-S or illite, where the illite occurs in 10 Å layer sequences with few (<15%) or no smectite-like layers. Other interstratified sequences with intermediate ratios of I-S were observed only as minor components representing local disorder or heterogeneity within dominant R=1 I-S or illite. Dong *et al.* (1997) emphasized the unique Si-Al ordering of the (R=1) I-S structure in contrast to alternating ideal smectite and illite layers, as discussed by Nadeau *et al.* (1985) and Ahn and Peacor (1986). In (R=1) I-S, Si-Al ordering is symmetric across the interlayer as implied by NMR data, rather than across the octahedral sheet as in ideal smectite and illite (Barron *et al.*, 1985; Altaner *et al.*, 1988; Jakobsen *et al.*, 1995). That requires that (R=1) I-S is thermodynamically stable relative to interstratified illite and smectite layers, as verified by recent calculations of structure energies (Stixrude, pers. comm.). That in turn implies discontinuities in the I-S sequence.

The continuous change in proportions of illite and smectite layers indicated by much XRD data appears to be inconsistent with the discontinuous changes in, and gaps between, discrete smectite, (R=1) I-S, and illite as observed by TEM. Dong and Peacor (1996) argued that these differences were in part related to packet disarticulation and the averaging of heterogeneous domains inherent in XRD data. However, the different conclusions regarding the nature of the interlayer sequences and transitions during illitization come from experiments performed on diverse sample occurrences; therefore, differences in the apparent nature of the I-S sequences may be real and a consequence of different geological parameters, rather than an artifact of the method of study. It is essential, therefore, to integrate both methodologies, XRD and TEM. Veblen *et al.* (1990) reported combined TEM and XRD observations on I-S. They noted that the proportions of illite- and smectite-like layers determined by the two methods were the same, a relation generally confirmed in several studies, even where the sequences of layers have been found to be different. Results similar to those of Dong *et al.* (1997) have been found by Tillick *et al.* (2001) and Yan *et al.* (2001), who studied illitization processes in volcanic rocks affected by hydrothermal alteration in New Zealand. They detected episodic alteration events where the dioctahedral phyllosilicates formed are smectite, (R=1) I-S, illite and mica. Similar relations have been observed in faulted shales (Yan *et al.*, 2001) and core from the Nankai Trench (Masuda *et al.*, 2001). In comparison with these studies, Bauluz *et al.* (2000) described, by TEM methods, progressive illitization from (R=1) I-S to illite through different I-S phases; however, a discontinuity exists between illite-rich I-S and illite.

The sequence of illite and smectite layers in interstratified I-S has important consequences for the mechanism of transformation (Altaner and Ylagan, 1997, and references therein). A discontinuous series involving discrete phases must occur via dissolution and neocrystallization in an Ostwald-step-rule-like sequence, whereas continuous layer sequences may occur by progressive, direct replacement of individual layers. The latter might be described as a "solid-state reaction", regardless if it occurs via an essential fluid at a near-atomic scale or not (Giorgetti *et al.*, pers. comm.). Therefore, in order to understand the transformation mechanisms, it is necessary to investigate sequences wherein the illitization process covers the complete range from smectite to illite.

In this study we have characterized, by SEM and TEM, the dioctahedral phyllosilicates from an altered rhyolitic hyaloclastite located at Ponza Island, Italy. Our purpose was to determine the characteristics of I-S interstratification caused by smectite illitization on undisturbed samples, especially to compare the textural relationships between the dioctahedral clay minerals, and the mechanism(s) of formation. Because the studied samples came from a more complete sequence which was also characterized by Ylagan *et al.* (1996, 2000) by XRD and other methods, this study permitted direct comparison of conclusions obtained independently by XRD and TEM.

GEOLOGICAL SETTING

The samples analyzed in this study are from Ponza Island, a volcanic island in the western Tyrrenian Sea. It is generally accepted that volcanism along the western margin of Italy resulted from extensional processes, possibly caused by either subduction (Peccerilli, 1985) or back-arc extension related to the formation of the Tyrrenian Sea (Malinverno and Ryan, 1986).

The volcanic deposits of Ponza are located on the boundary between two volcanic provinces in western Italy: the silica-saturated rhyolite and rhyodacite typical of the Tuscan Magmatic Province and silica-undersaturated trachyte and phonolite which characterize the Roman-Campanian province. The volcanic deposits of Ponza are regionally heterogeneous, with rhyolitic hyaloclastite (~4.5 Ma, Barbieri *et al.*, 1967; Savelli, 1983, 1987) common in the north, and younger trachytic pyroclastic flows and tuff cones (~1.1 Ma, Barbieri *et al.*, 1967; Savelli, 1983, 1987) in the south. Thus, the geological history of this island appears to have been dominated by two distinct periods of volcanism, each equivalent both chronologically and geochemically to more regionally extensive volcanic events.

Because our study is concerned with the alteration of materials from the earlier volcanic stage, it is important to consider the sequence of subsequent volcanic activity and related hydrothermal alteration. The first volcanic stage involved emplacement of massive dikes and a thick, highly brecciated, rhyolitic hyaloclastite which crops out over most of Ponza and Gavi Islands (Pichler, 1965, Barberi *et al.* 1967). The hyaloclastite was

Table 1. Dioctahedral clays identified by XRD in selected samples for this study, along with ordering in I-S phases, *cis*-vacant sites (P*cv*), proportion of unrotated layers (P_0), and average thickness in nm (*N*). These XRD-determined data were reported by Ylagan (1996) and Ylagan *et al.* (1996, 2000).

Sample	Size-fraction	Clay	R	P*cv*	P_0	*N*
93-6-8C	<0.5 μm	Sm	0	0.85	0.75	1.15
93-6-9Q	<0.1 μm	I-S (59% I)	1	0.60	0.90	2.29
93-6-8N	<0.5 μm	I-S (90% I)	3	0.33	0.95	5.13
	<0.1 μm	I-S (82 % I)	2.5	–	–	–
93-6-10A	<0.5 μm	Illite		0.10	1	11.8
	<0.1 μm	I-S (92% I)	3	–	–	–

probably formed at 4.5 Ma by the submarine eruption of silicic lavas, which brecciated due to rapid cooling (Pichler, 1965; Barberi *et al.*, 1967; Carmassi *et al.*, 1983).

PREVIOUS WORK ON THE PONZA BENTONITE

Numerous studies of the mineralogy of the Ponza bentonite indicate that smectite is typically the dominant mineral. Other reported minerals include I-S, illite, opal-C, mordenite, kaolinite, sulfides (pyrite, chalcopyrite, sphalerite and galena) and sulfates (Lupino, 1954; Güven and Grim, 1972; Grim and Güven 1978; Lombardi and Mattias, 1981; Pozzuoli, 1988; Passaglia *et al.*, 1995). Smectite has a ribbon-like morphology on the basis of TEM images (Güven and Grim, 1972; Grim and Güven, 1978). Pozzuoli (1988) found that although smectite is dominant in most outcrop samples, significant illitization occurs with increasing depth (>65 m). He estimated a range of alteration temperatures from 127 to 368°C. Ylagan (1996) and Ylagan *et al.* (1996) studied in detail the illitization process associated with the hydrothermal alteration in the rhyolitic hyaloclastite, describing a transformation from turbostratic smectite to interstratified *cis*- and *trans*-vacant, $1M_d$ I-S, $1M$ illite, and then to $2M_1$ illite. According to this study, I-S composition changes progressively during illitization, evolving toward a phengitic end-member with ~0.89 fixed interlayer cations per half unit-cell.

Most studies concluded that the bentonite formed as a result of hydrothermal processes. However, a more recent study (Passaglia *et al.*, 1995) suggests that alteration occurred in an open hydrologic system in which meteoric waters reacted with the hyaloclastite, as influenced by a high geothermal gradient. Other studies have also concluded that alteration of the bentonite involved meteoric waters, on the basis of the chemical composition of exchangeable cations (Pozzuoli, 1988).

SAMPLE DESCRIPTIONS

The samples represent a complete range of illitization, and were studied previously by Ylagan (1996) and by Ylagan *et al.* (1996, 2000), The unaltered hyaloclastite is a volcanic breccia with clasts of vesiculated obsidian in a matrix dominated by pumice lapilli. Ylagan described four alteration zones: the argillic zone, characterized by smectite, highly disordered opal-CT and abundant fresh pumice remains; the propylitic zone, characterized by randomly and short-range ordered R=0 and R=1 I-S with 10–82% I, mordenite, opal-C, and uncommon feldspar and quartz; the silicic zone, characterized by long-range ordered R=3 I-S with ⩾90% I, illite, quartz, feldspar, albite, and minor jarosite; and the sericitic zone, where the mineral assemblage is dominated by I-S with >65% I, illite, quartz and minor feldspar, pyrite and jarosite.

The four alteration zones are represented by samples 93-6-8C, 93-6-9Q, 93-6-8N and 93-6-10A, chosen for TEM analysis as representative of a much larger number of samples characterized by XRD. Using calculated XRD patterns, Ylagan (1996) determined I-S ordering, the proportion of *cis*-vacant sites (P*cv*) and degree of rotational disorder. These results are reported in Ylagan (1996) and Ylagan *et al.* (1996, 2000), and brief summaries for the selected samples are given in the following and Table 1.

Smectite with no interstratified illite was the only clay mineral detected in sample 93-6-8C (argillic zone). There is a high proportion of *cv*-sites relative to *trans*-vacant (*tv*) sites (P*cv*=0.85), and a high degree of rotational disorder (P_0= 0.75). Based on atomic force microscopy (AFM), the mean thickness of powdered particles is 1.15 nm.

Sample 93-6-9Q (propylitic zone) contains (R=1) I-S (59% illite), with P*cv*=0.6 indicating that the *cv*/*tv* ratio decreased in comparison with sample 93-6-8C, and P_0=0.9 (smaller rotational disorder than in smectite of sample 93-6-8C). The average thickness is 2.29 nm.

The <0.5 μm and <0.1 μm size-fractions of sample 93-6-8N (silicic zone) contain (R=3) I-S (90% illite) and (R=2.5) I-S (82% illite), respectively. P*cv* =0.33 and P_0 = 0.95. The mean particle thickness is 5.13 nm.

The <0.5 μm and <0.1 μm size-fractions of sample 93-6-10A (sericitic zone) contain illite and (R=3) I-S (92% illite), respectively; the P*cv* (0.1) and P_0 (1) values indicate that it consists of ordered *tv*-illite. The mean illite particle thickness is 11.8 nm.

https://doi.org/10.1346/000986002760832766 Published online by Cambridge University Press

The complete sequence of samples studied by Ylagan indicates that as illitization proceeds, I-S samples from Ponza Island change systematically from *cv* to *tv* and n·120° rotational disorder decreases. These results indicate that during illitization, I-S from Ponza Island changes progressively from turbostratic, *cv*-smectite to 1*M tv*-illite, with a continuous increase in the proportion of illite-like layers. In addition, the two most illitic samples from the sericitic zone also contain authigenic $2M_1$ illite (5–15%).

TEM PROCEDURES

Samples were treated with L. R. White resin following the procedure of Kim *et al.* (1995) in order to prevent collapse of smectite-like interlayers in the vacuum of the ion mill and TEM, as well as to facilitate differentiation of illite and smectite interlayers in TEM images. Great care was taken to avoid direct contact with water during sample preparation in order to avoid expansion of smectite and resultant sample damage. Sticky wax-backed thin-sections were prepared with surfaces normal to bedding, and first examined by optical microscopy. Typical areas were removed for SEM and TEM observations via attached Al washers, thinned in an ion mill and carbon coated. The SEM observations were made with an Hitachi S570 instrument. The TEM data were obtained using a Philips CM-12 scanning-transmission electron microscope (STEM). Both the SEM and STEM were fitted with Kevex Quantum solid-state detectors and computer systems, the detector having a boron-composite window permitting analysis of low atomic number elements. The STEM was operated at 120 kV and a beam current of 20 μA. Through-focus series of images were obtained from 1000 Å underfocus (approximate Scherzer defocus) to 1000 Å overfocus, in part to obtain optimum contrast in I-S ordering (overfocus). However, because initial focus was controlled manually by minimizing contrast, small deviations from exact underfocus or overfocus numbers were inevitable. A camera length of 770 mm and a selected-area aperture 10 μm in diameter were used to obtain SAED area. The EDS data were processed using Kevex software, with resultant intensity ratios being corrected with k values determined for well-characterized samples, following the methods of Jiang and Peacor (1993). The concentration ratios were then normalized to 22 negative charges for clay minerals. Errors of reported analytical values are ~3–5% of the amount present.

RESULTS

Scanning electron microscopy

Back-scattered electron (BSE) images of the four samples are presented in Figure 1. Sample 93-6-8C (Figure 1a,b) has a typical texture formed by obsidian clasts partially replaced by smectite. The clasts are embedded in a matrix of smectite-like composition, which probably originally comprised small pumice lapilli. The EDS analyses of the replaced clasts indicate a large Si content and minor Al, Mg, K, Na, Ca and Fe (in decreasing concentrations), whereas the fine-grained matrix has larger Al, Mg and Fe contents, both being compatible with major proportions of smectite. Minor authigenic calcite, apatite, barite and Fe-Ti oxides were also identified by EDS analyses.

As illustrated in Figure 1c,d, sample 93-6-9Q consists of pseudomorphs of clast fragments replaced by phyllosilicates with fibrous mordenite lining pores, with minor quartz and K-rich feldspar. Alteration to clay minerals preserved vesicular textures, but K-feldspars are unaltered, the EDS analyses showing that they have very small Na components. The EDS analyses of the clay show an average composition rich in Si, Al and K, with minor Ca and Na. This implies the presence of dominant dioctahedral clay minerals, in contrast to the mordenite, whose EDS spectrum shows that it is rich in Si, Al and Na. Sample 93-6-8N consists of clasts completely pseudomorphed by illite-like phases (Si-, Al-, K-rich phases), K-feldspar, albite, quartz and jarosite (Figure 1e). In the most altered sample, 93-6-10A (Figure 1f,g,h), obsidian clasts and lapilli matrix have been completely replaced by illitic clays.

Petrographic photomicrographs and SEM images reported by Ylagan *et al.* (1996) similarly showed direct alteration of pumice to I-S and fibrous mordenite, with evidence of dissolution of pumice. Mordenite lines vesicles filled by euhedral feldspar, and plagioclase feldspar was replaced by illitic I-S (see Figures 8 and 9 in Ylagan *et al.*, 1996). Ylagan *et al.* also showed euhedral lath-like and hexagonal shapes of authigenic phyllosilicates as recorded in TEM images in size-separated samples (see Figure 10 in Ylagan *et al.*, 1996).

Transmission electron microscopy

The TEM observations of the four samples are described below in order of increasing degree of illitization.

Sample 93-6-8C (smectite). As shown in Figure 2, this sample contains both volcanic glass and smectite, and it is apparent from the images that the glass is in the process of being replaced by smectite (Figure 2). The smectite is characterized by discontinuous, wavy fringes, with d-spacings from 10 to 13 Å (Figure 2b), depending on the degree of dehydration and layer collapse caused by interaction with the electron beam or the TEM or ion-mill vacuums. There are abundant layer terminations. The SAED patterns show diffuse low-order 00l reflections, and non-00l reflections are ill-defined, non-periodic and diffuse parallel to **c*** (Figure 2c). The AEM-determined compositions of such smectite show octahedral cation contents close to 2 (2.08), indicating a dioctahedral character (Table 2). Interlayer charges are

https://doi.org/10.1346/000986002760832766 Published online by Cambridge University Press

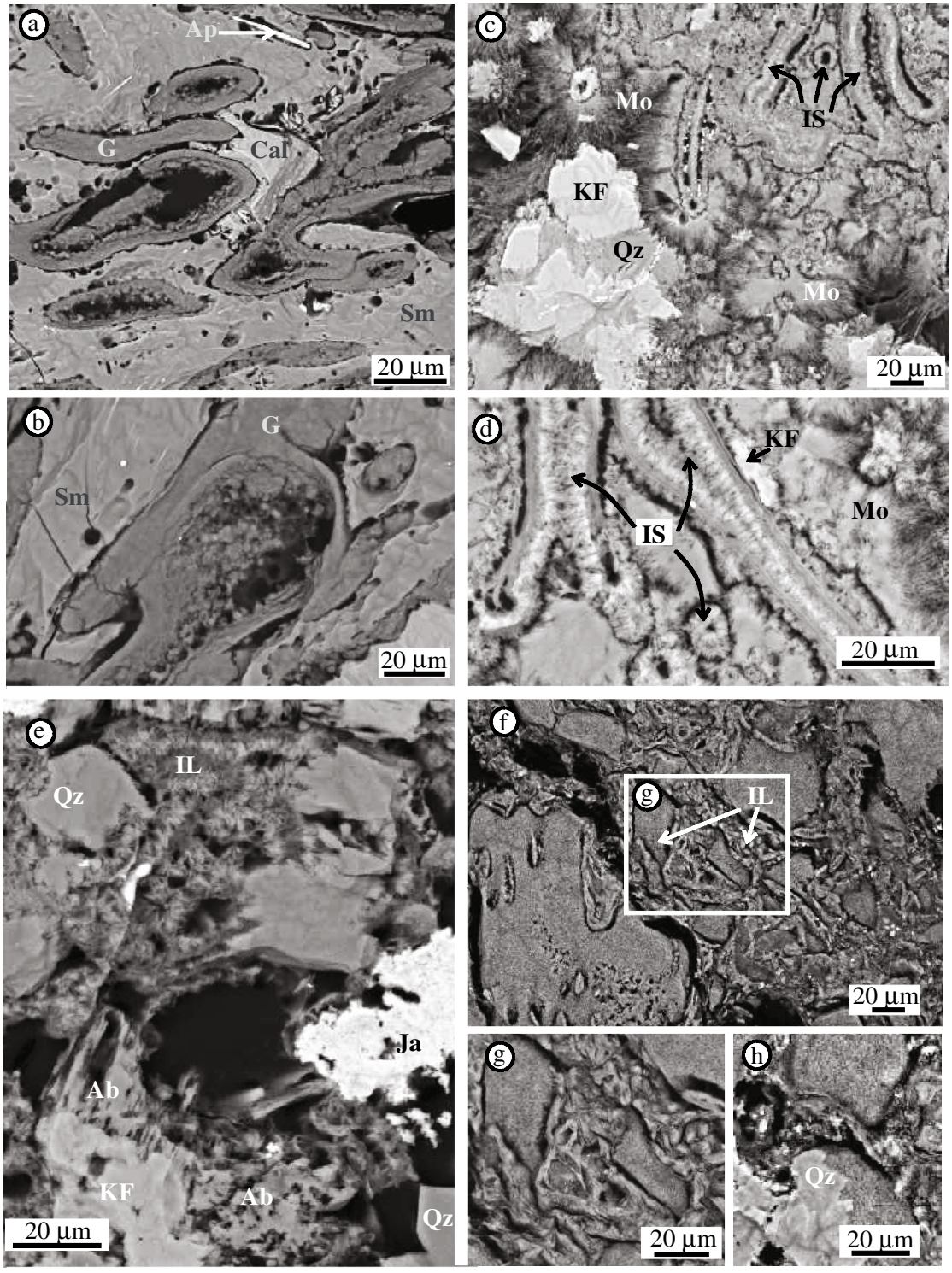

Figure 1. BSE images from ion-milled areas of samples from the different alteration zones: (a, b) Argillic zone, sample 93-6-8C: obsidian clasts (G) partially replaced by smectite embedded in a smectite-like matrix (Sm), adjacent to authigenic calcite (Cal) and apatite (Ap). (c, d) Propylitic zone, sample 93-6-9Q: I-S pumice pseudomorphs replaced by IS phases, hairy mordenite filling pores (Mo) and authigenic quartz (Qz) and K-feldspar (KF). (e) Silicic zone, sample 93-6-8N, illite-like phases (IL) filling pores and replacing corroded albite feldspar (Ab) adjacent to authigenic quartz, K-feldspar (KF) and jarosite (Ja). (f, g, h) Sericitic zone, sample 93-6-10A, illitic phases (IL) lining pores and irregular cavities.

https://doi.org/10.1346/000986002760832766 Published online by Cambridge University Press

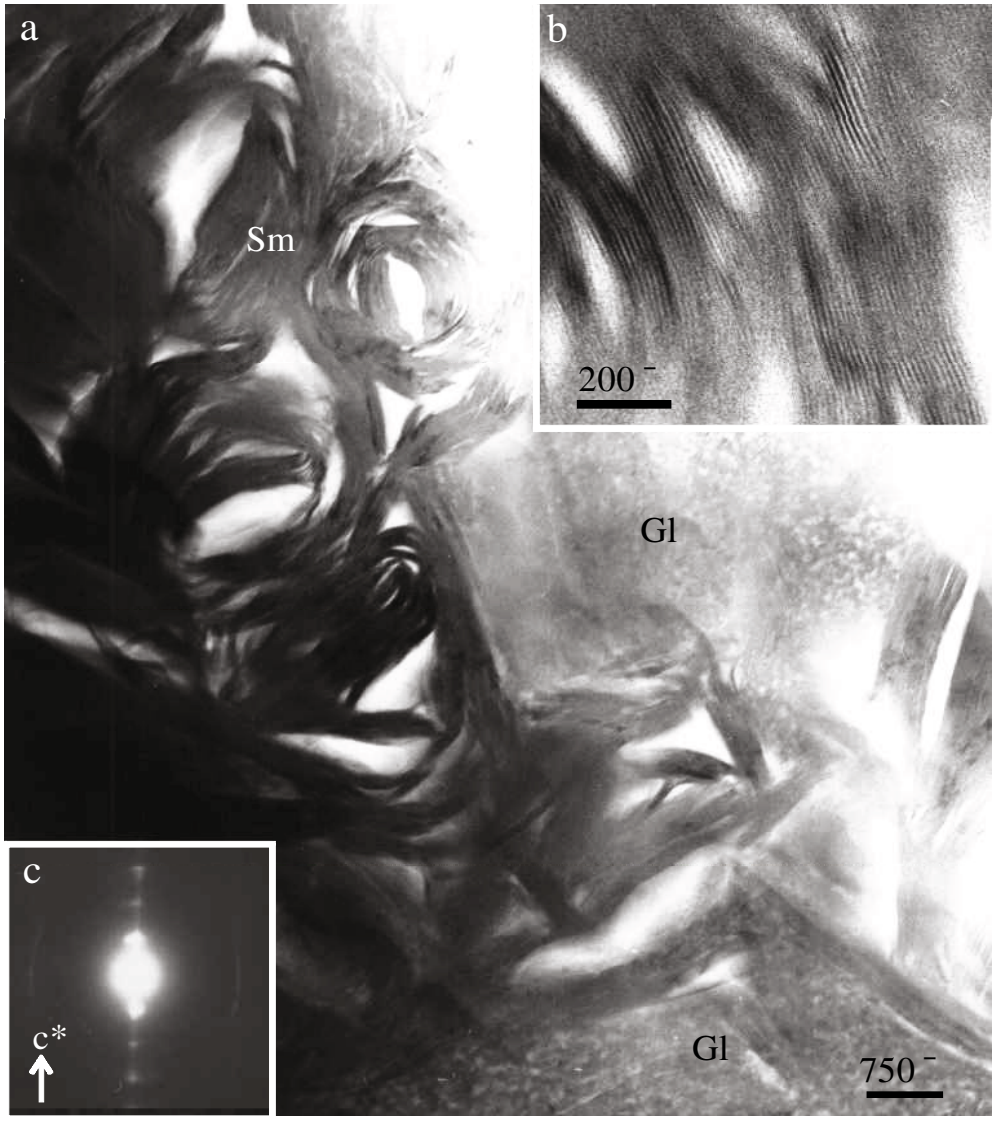

Figure 2. TEM images of sample 93-6-8C. (a) Low-magnification image showing the typical curved lens-shaped morphology of smectite (Sm), with no preferred orientation, surrounding relatively featureless amorphous cores (Gl). (b) Wavy and discontinuous lattice fringes of smectite, with spacings from 10 to 13 Å, depending on the degree of dehydration and layer collapse caused by interaction with the electron beam or by the TEM vacuum. (c) SAED pattern corresponding to smectite, with diffuse low-order 00*l* reflections and ill-defined and non-periodic non-00*l* reflections with diffuseness parallel to **c***.

small and typical of smectite (0.45), with the interlayers containing Na, Ca and K. The analyses also indicate that the tetrahedral charge is less than the octahedral charge, implying that the smectite is montmorillonite.

Smectite packets exhibit a curved (sometimes circular or semi-circular) lens-shaped morphology in TEM images, with no preferred orientation. Curved packets of smectite with a discontinuous circular shape are commonly observed to surround relatively featureless cores. The cores give no SAED patterns, consistent with amorphous material. However, it is also possible that rapid degradation from electron-beam interaction causes the core material to become non-diffracting. This is a common occurrence in defect-rich material, so that such material may actually have a partially ordered structure which cannot be detected within the present limits of SAED observations (*e.g.* Masuda *et al.*, 1996). The AEM analyses of this glassy material are similar to those of smectite, but they show enrichment in Si and larger variability in element concentrations (Table 3), probably due to the variable and transitional degree of alteration of glass to smectite. Lattice fringes corresponding to smectite were observed occasionally within these glass-like domains. The collective data imply that the non-

https://doi.org/10.1346/000986002760832766 Published online by Cambridge University Press

Table 2. Compositions of dioctahedral phyllosilicates of samples 93-6-8C, 93-6-9Q, 93-6-8N and 93-6-10A as determined from AEM data. Analyses have been normalized to 22 negative charges.

	93-6-8C (smectite)		93-6-9Q (R1 I-S)		93-6-8N (highly illitic I-S)		93-6-10A (illite)		93-6-10A (mica)	
Si	3.88	3.74 – 4.07	3.61	3.44 – 4.07	3.41	3.22 – 3.58	3.36	3.26 – 3.52	3.34	3.23 – 3.44
Al^{IV}	0.13	0.00 – 0.26	0.39	0.00 – 0.56	0.59	0.44 – 0.78	0.64	0.48 – 0.74	0.66	0.56 – 0.77
Al^{VI}	1.47	1.37 – 1.58	1.58	1.44 – 1.66	1.63	1.54 – 1.80	1.72	1.66 – 1.77	1.68	1.58 – 1.81
Fe	0.18	0.13 – 0.25	0.24	0.19 – 0.29	0.27	0.18 – 0.49	0.04	0.00 – 0.11	0.08	0.03 – 0.14
Mg	0.42	0.33 – 0.50	0.33	0.28 – 0.39	0.19	0.00 – 0.29	0.31	0.22 – 0.45	0.27	0.17 – 0.38
Ti	0.01	0.00 – 0.02	0.00	0.00 – 0.04	0.00	0.00 – 0.02	0.00	0.00 – 0.02	–	–
K	0.10	0.09 – 0.17	0.37	0.17 – 0.50	0.66	0.52 – 0.86	0.69	0.56 – 0.80	0.83	0.70 – 1.04
Na	0.16	0.00 – 0.35	0.06	0.00 – 0.16	0.12	0.00 – 0.34	0.06	0.00 – 0.19	0.06	0.00 – 0.17
Ca	0.10	0.07 – 0.12	0.05	0.00 – 0.12	–		–		0.01	0.00 – 0.03
Σoct	2.08	1.90 – 2.16	2.15	1.97 – 2.21	2.09	1.97 – 2.19	2.08	2.03 – 2.14	2.04	1.97 – 2.15
Int. ch.	0.45	0.26 – 0.63	0.53	0.40 – 0.70	0.78	0.67 – 1.00	0.75	0.65 – 0.83	0.91	0.52 – 1.14

Σoct= sum of octahedral cations; Int. ch. = interlayer charge (ΣK+Na+2Ca)

diffracting cores central to smectite packets consist of a poorly-ordered, but chemically similar, precursor to crystalline smectite.

Sample 93-6-9Q ([R=1] I-S, 59% illite). The TEM images show the occurrence of fibrous mordenite crystals (Figure 3a) and I-S (Figure 3b). The mordenite appears as euhedral 70 – 100 nm thick crystals, and its morphology implies that it precipitated directly from interstitial fluids. The I-S displays curved structures, with preservation of vesicular textures similar to the smectite from sample 93-6-8C. Boundaries between individual packets are diffuse and appear to grade into the matrix. Fringes show the alternating dark and light contrast typical of mixed-layer I-S (Figure 4) (Guthrie and Veblen, 1989a,b, 1990; Veblen *et al.*, 1990). Moreover, these fringes have spacings (21 to 22 Å periodicity) characteristic of the sum of illite- and smectite-like layer spacings in (R=1) I-S (Kim *et al.*, 1995; Dong *et al.*, 1997). We use the term I1 for such individual units, as described above. Additionally, there are some layers comprising I2 (31 to 32 Å periodicity), I3 (41 to 42 Å periodicity) units (Figure 4b). The SAED patterns display relatively high orders of 00l reflections with $d_{001} \approx 10$ Å (Figure 4c). Diffuseness both parallel and normal to **c*** is present. Diffuseness normal to **c*** is caused by small variations in layer orientations, whereas the more marked diffuseness parallel to **c*** is caused by mixed-layering. Non-00*l* reflections are ill-defined, non-periodic and diffuse parallel to **c***, implying that stacking is generally random, but with local coherency with respect to scattering of electrons. Such SAED patterns have commonly been found to be diagnostic of $1M_d$ polytypism.

The AEM analyses of I-S and mordenite crystals are listed in Tables 2 and 3. The I-S chemical compositions show that the sum of octahedral cations approximates ideal dioctahedral occupancy of 2.0 (2.15). Interlayer cations include K, Na and Ca (in decreasing concentrations). Mordenite compositions (normalized to 96 oxygen atoms) show that the exchangeable cation is predominantly Na, with minor K and Ca.

Sample 93-6-8N ([R=3] I-S, 90% illite). The TEM images show illite crystals with variable orientation (Figure 5a). Most of the crystals are 10 to 15 nm thick and have relatively straight boundaries which are more clearly defined than those of the previous sample. High-magnification images show they are mainly formed by straight (001) fringes with 10 Å spacings (Figure 5b), although uncommon wavy lattice fringes with slightly larger spacings (~11 Å) occur and probably correspond

Table 3. Chemical composition (wt.%) of glasses occurring in the smectite-rich sample (93-6-8C), mordenite corresponding to I1-rich sample (93-6-9Q), and mordenite composition normalized to 96 oxygen atoms.

	Glasses (*n*=6)		Mordenite (*n*=3)			Mordenite (*n*=3)	
%	average	st.dv.	average	st. dv.		average	st. dv.
Na_2O	4.20	(4.23)	7.91	(1.02)	Na	8.41	(1.09)
MgO	2.56	(0.50)	1.65	(0.46)	Mg	1.36	(0.38)
Al_2O_3	21.34	(5.25)	25.53	(0.52)	Al	16.52	(0.34)
SiO_2	65.37	(3.86)	59.07	(2.26)	Si	32.47	(1.24)
K_2O	2.25	(1.14)	3.03	(1.96)	K	2.13	(1.38)
CaO	0.80	(0.42)	2.08	(0.43)	Ca	1.22	(0.25)
TiO_2	0.36	(0.64)	–		Ti	–	
Fe_2O_3	3.13	(1.24)	0.74	(1.04)	Fe	0.30	(0.43)

https://doi.org/10.1346/000986002760832766 Published online by Cambridge University Press

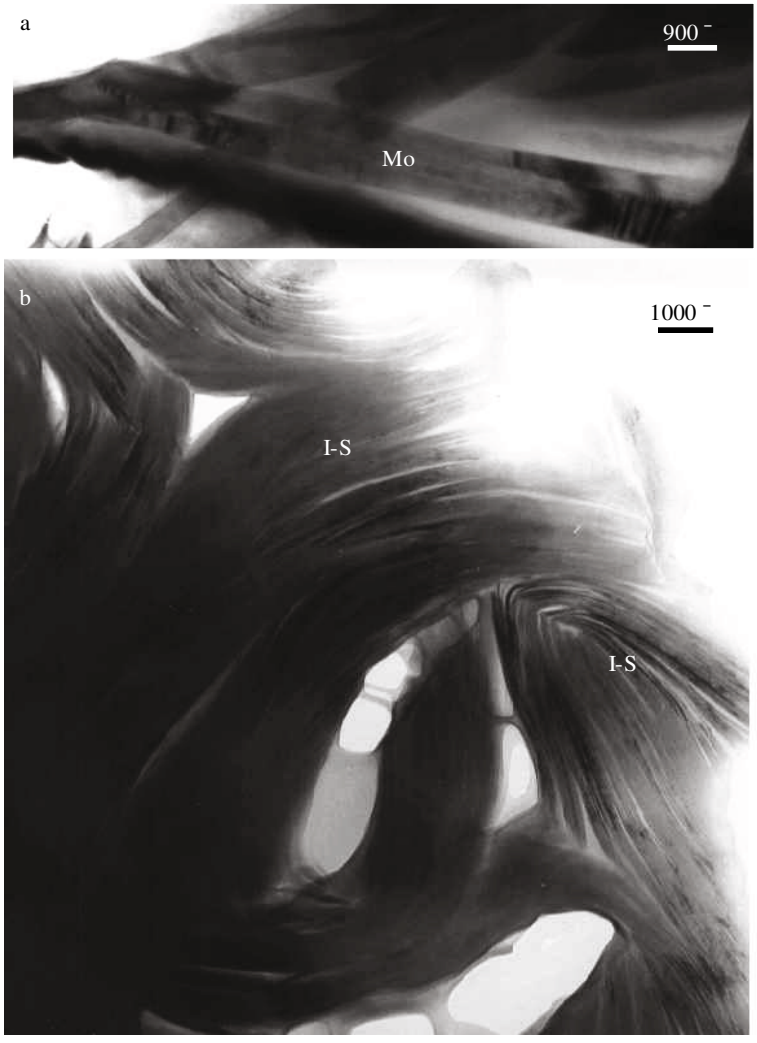

Figure 3. TEM images corresponding to sample 93-6-9Q. (a) Euhedral mordenite crystals. (b) Low-magnification image of I-S phases, showing curved textures.

to smectite layers. These wavy fringes are often associated with lens-shaped voids as consistent with partial collapse caused by the TEM vacuum despite sample treatment with L. R. White resin. According to these images, this sample is composed of illite crystals with local regions of highly illitic I-S.

The SAED patterns display relatively high orders of 00l reflections with $d_{001} \approx 10$ Å (Figure 5c), with diffuseness normal and parallel to **c*** commonly present. Non-00*l* reflections are ill-defined, non-periodic and diffuse parallel to **c***, implying that stacking is generally random, but with local coherency. In some SAED patterns, the 0*kl* reflections are better defined, indicating a higher degree of order; the average pattern is, however, characteristic of $1M_d$ polytypism.

The AEM analyses of these materials show that they are dioctahedral, with octahedral cation contents close to the ideal value of 2 (2.09), with interlayer charges similar to that of illite (0.78), and with K as the dominant interlayer cation; no Ca was detected.

Sample 93-6-10A ([R=3] I-S, >92% illite + 5–15% $2M_1$). Low-magnification images show the presence of two different types of illite-like phases (Figure 6). Because each kind occurs separately, SAED patterns, high-resolution images and microanalyses could be correlated directly for each kind:

(1) Crystallites which appear to have replaced obsidian clasts consist of straight and defect-free lattice fringes with constant 10 Å spacings, displaying uniform contrast, consistent with relatively constant orientation. They comprise 10–15 nm thick, parallel- to subparallel packets with relatively well-defined boundaries (Figure 7a). The corresponding SAED patterns show well-defined 00*l* reflections with d_{00l} = 10 Å (Figure 7b). Non-00*l* reflections are generally non-

https://doi.org/10.1346/000986002760832766 Published online by Cambridge University Press

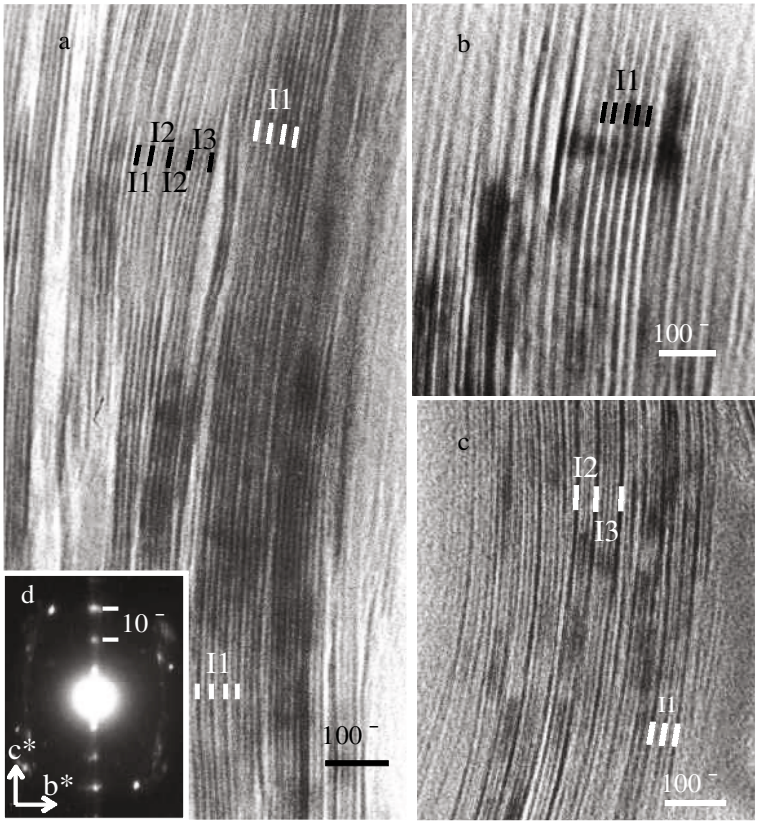

Figure 4. Lattice-fringe images of I-S occurring in sample 93-6-9Q. (a) Typical area rich in I1 units with 21–22 Å periodicity. These spacings suggest that treatment with L.R. White resin prevented the complete collapse of smectite in the vacuum of the TEM. The fringes are relatively straight compared to those of smectite; some layer terminations occur. (b) I*n* units with $n>1$, which are uncommon relative to I1 units. (c) Typical SAED pattern corresponding to I-S phases, with relatively high orders of 00*l* reflections with $d_{001} \approx 10$ Å. Diffuseness both parallel and normal to **c*** is present. Non-00*l* reflections are ill-defined, non-periodic and diffuse parallel to **c***, implying that stacking is generally random, but with local coherency with respect to scattering of electrons. Such SAED patterns are diagnostic of $1M_d$ polytypism.

periodic parallel to **c***, diffuse, and ill-defined, and therefore are typical of $1M_d$ polytypism. The AEM analyses indicate that they are dioctahedral, the octahedral occupancy being close to 2 (2.08). The dominant interlayer cation is K, and no Ca was detected. The interlayer charge is 0.75. These collective TEM and AEM data show that the crystals are illite which contains no other kinds of interstratified layers. There is significantly less Fe in comparison with illitic phases of sample 93-6-8N.

(2) Elongate crystals as seen in cross-section with variable orientation are 25–35 nm thick, considerably thicker than the illite (Figure 8a,b). Lattice fringes are straight and defect free. The SAED patterns show that they have well ordered 2-layer polytypism, inferred to be of $2M_1$-type (Figure 8c) as normal for muscovite. Compositions are typical of dioctahedral micas, and enrichments in Si (3.34 p.f.u.) and Mg (0.27) relative to muscovite indicate a phengite substitution. Potassium is dominant in the interlayer and its proportion is greater than in illite. The interlayer charge is close to the ideal value of 1.0 (0.91). These collective data are consistent with mature muscovite with a large phengite component. The XRD patterns of this sample suggested a small proportion of $2M_1$ mica, <15%, but the TEM images show that the mica is an important component of the sample although its distribution is not homogeneous.

DISCUSSION

Smectite to mixed-layer I-S to illite to mica transition

Overview. In studying bentonite samples from Ponza by XRD, Ylagan (1996) detected an illitization sequence which was apparently continuous from smectite through I-S phases to illite. The TEM data for two of the four samples described herein are in complete agreement with the data of Ylagan (1996), but are significantly different for two others, with TEM data implying a discontinuous sequence of phases. Characterization of samples 93-6-8C (argillic zone) and 93-6-9Q (propylitic zone) by both TEM and XRD data are nearly identical. The only phyllosilicate present in sample 93-6-8C is

https://doi.org/10.1346/000986002760832766 Published online by Cambridge University Press

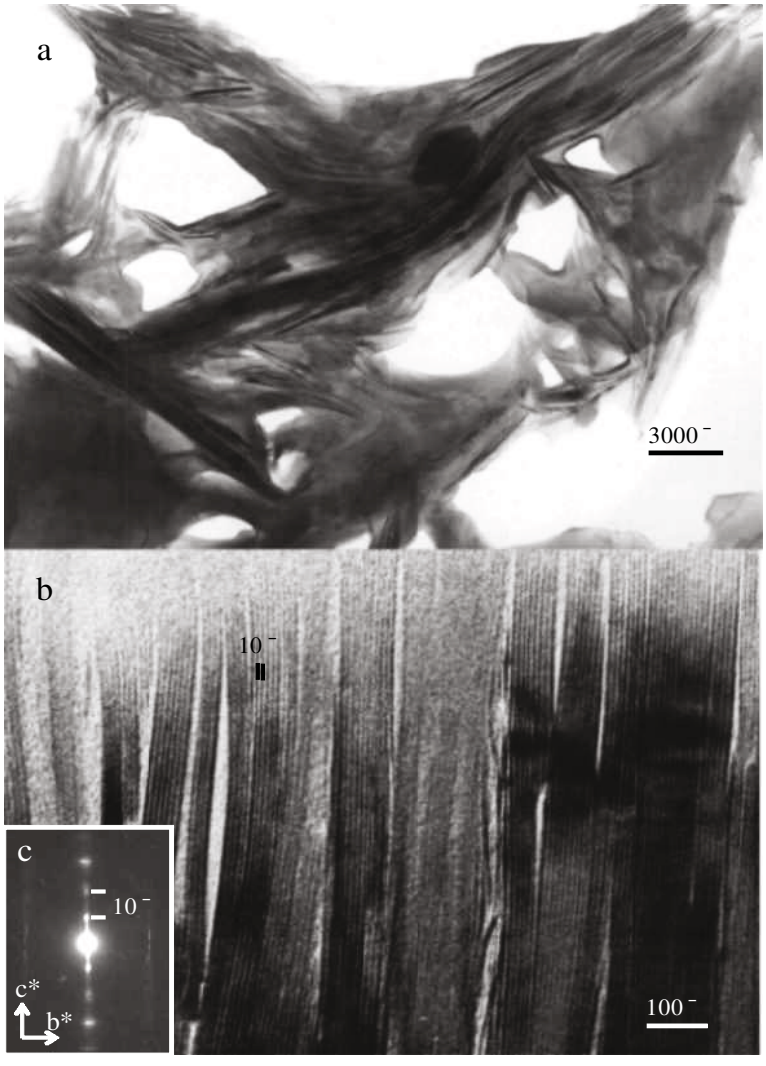

Figure 5. TEM images of sample 93-6-8N. (a) Low-magnification image of sample 93-6-8N showing illitic crystals with variable orientation. (b) Lattice-fringe images of highly illitic I-S, consisting of straight 001 fringes with 10 Å spacings. Uncommon wavy lattice fringes with slightly larger d-values (~11 Å) occur which probably correspond to smectite layers. (c) Typical SAED pattern of I-S phases, with relatively high orders of 00l reflections with $d_{001} \approx 10$ Å, with diffuseness normal and parallel to **c***. Non-00l reflections are ill-defined, non-periodic and diffuse parallel to **c***, as characteristic of $1M_d$ polytypism.

smectite. Sample 93-6-9Q consists only of (R=1) I-S by XRD, with TEM images showing that it is largely composed of I1 units with a small proportion of In units with n>1. Observation of the latter In units is compatible with > 50% illite-like layers (59%) as detected by XRD.

The XRD patterns from sample 93-6-8N (silicic zone) implied that it consists of (R=3) I-S or (R=2.5) I-S, depending on the crystallite size. However, TEM lattice-fringe images show that it consists mainly of highly illitic I-S which does not contain I3 units, and that does not correspond, on average to (R=3) I-S, in part because the proportion of smectite-like layers is too small to produce R3 ordering. The most highly altered sample, 93-6-10A, (sericitic zone), gives XRD patterns interpreted to correspond to $1M$ (R=3) I-S and minor $2M_1$ illite (<15%). Although the TEM results reflect the coexistence of illite and mica, the mica is an important component of the sample and the illite is $1M_d$. No $1M$ illite or $1M$ mica were observed, and no smectite was detected. Such comparisons of XRD and TEM data are discussed separately for each sample, below.

Lack of R3 ordering. Both the XRD and TEM data imply a prograde trend from sample 93-6-8C to 93-6-10A, but there are differences in the characteristics of the intermediate phases. One of the differences is the lack of recognizable R3 (or I3 units) order in TEM images of sample 93-6-8N. The sample has very low expandability. As a result of the lack of clearly-defined smectite-like layers, and the presence of straight layers with d = 10 Å,

https://doi.org/10.1346/000986002760832766 Published online by Cambridge University Press

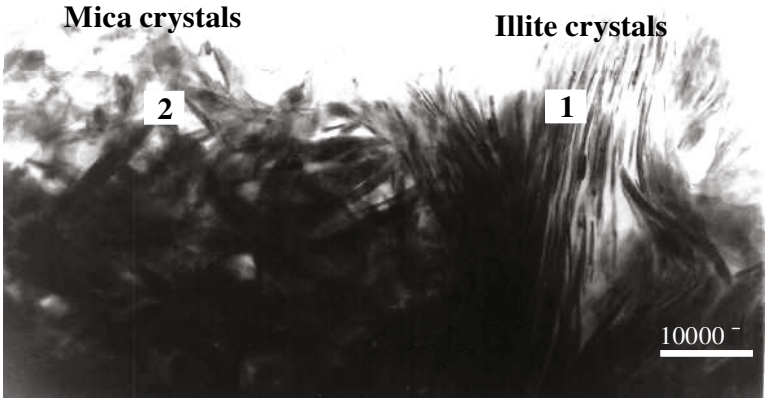

Figure 6. Low-magnification image of sample 93-6-10A showing two different types of crystals: (1) illite and (2) mica.

it was not possible to identify I*n* units with $n \approx 3$. The TEM images thus imply that where I*n* can be identified it has $n>>>3$. On the other hand, TEM images of sample 93-6-10A show that separate packets of mica and illite coexist, the latter having the ideal characteristics of illite with no interstratified smectite-like layers. This discrepancy in the estimation of the proportion of smectite layers by the two methods may be due to a number of factors, including: (1) The differences in expandability of interlayers as affected by the different chemicals used in specimen preparation for XRD and TEM, in response to interlayers of a range of net negative charges, may result in different relative expandabilities of interlayers. Unpublished data of Kao (pers. comm.) imply that L.R. White resin does not diffuse into interlayers, but only acts to maintain the dimensions of the untreated sample, in contrast to the action of ethylene glycol, for example. (2) Interpretations of XRD data depend on calculations based on models of layer sequences which may not correctly reflect the local ordering which is observed directly by TEM. (3) The TEM observations are made on uncleaved samples, whereas XRD observations are usually carried out on samples which are disarticulated and chemically treated. Such treatment may cause preferential separation of I-S along smectite interfaces. Even though relative proportions of layers are unchanged, assuming that interparticle diffraction occurs, such reconstitution must result in changes in the

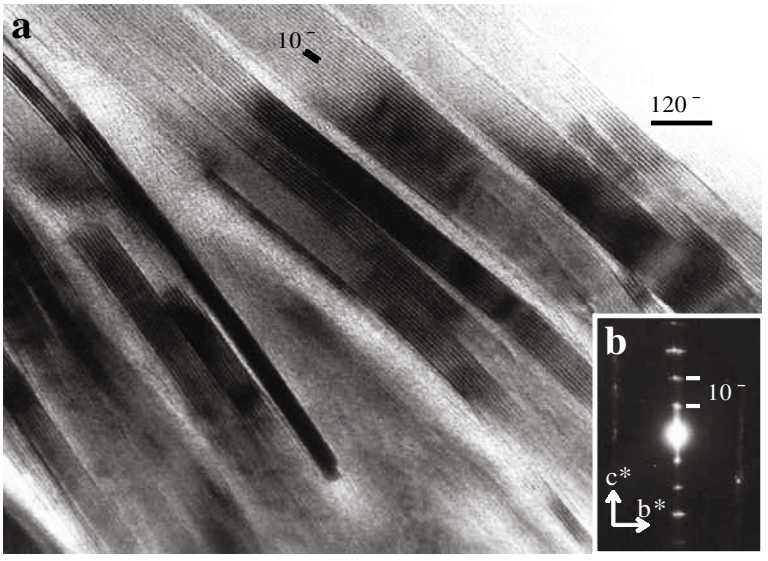

Figure 7. (a) Lattice-fringe image of illite crystals of sample 93-6-10A. These areas consist of 10–15 nm thick, parallel and subparallel packets with relatively well-defined boundaries. The image shows defect-free lattice fringes with constant 10 Å spacings indicating that these layers were not affected by L. R. White resin. (b) Characteristic SAED pattern of illite crystals corresponding to $1M_d$ stacking.

https://doi.org/10.1346/000986002760832766 Published online by Cambridge University Press

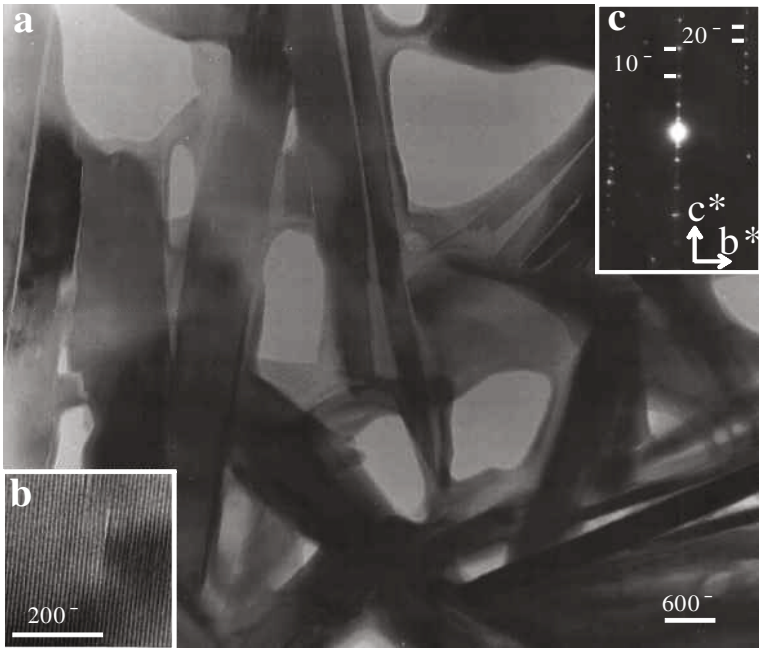

Figure 8. (a) TEM image of a mica crystal-rich area. Crystals have variable orientation and there is abundant pore-space. (b) Lattice-fringe image of mica crystals. They have straight 10 Å layers and show the typical mottled appearance of mica. (c) Typical SAED pattern of micas, showing high orders of 00*l* reflections with $d_{001} \approx 10$ Å. Non-00*l* reflections are well defined and periodic (20 Å), indicating that they correspond to a well-ordered 2-layer polytype, probably $2M_1$. The 00*l* row has weak reflections showing 20 Å periodicity due to dynamical diffraction.

interlayer relations, in part related to cleavage along some illite-like interlayers. (4) As pointed out by Guthrie (pers. comm.), it is sometimes not possible to obtain images which permit identification of smectite and illite layers. It is possible that lack of identification may occur in layer sequences of certain types, thus biasing the TEM results. These explanations are, of course, all speculative and without direct confirmation, but they suggest directions in which future research may be focused.

On the other hand, the AFM results of Ylagan (1996) for this same sample 93-6-8N support our TEM data since his study shows that the mean thickness of I-S stacks is, in most cases, >5 nm, indicating an ordering R>5. In addition, we are not aware that any TEM study has described R3 ordering (20–30% smectite) despite the large numbers of such studies of I-S sequences; *e.g.* TEM observations similar to those of this study were reported by Dong *et al.*, (1997) for a sample from Zempleni, Hungary which was kindly supplied by J. Środoń. Their results, which showed the presence of illite and (R=1) I-S but no I3 I-S, were inconsistent with the XRD data reported by Środoń (1984) having concluded it was composed of illite and (R=3) I-S.

The apparent disagreement among XRD results and those of AFM and TEM for material identified as (R=3) I-S by XRD is probably due to the fact that AFM and TEM methods may more accurately characterize long-range ordering than XRD. For example, XRD patterns of R3, R4 or R5 ordering schemes are very similar in illite-smectite samples that are highly illitic (>90%) and have large crystallite distributions. In these circumstances, I4 and I5 units should be dominant, but XRD results would be interpreted as R3 when the number of I3 units may be in the extreme minority. The data of this study suggest that where XRD data imply R=3 ordering, the actual ordering may be greater and therefore XRD may underestimate the actual long-range sequencing of illite layers observed by TEM or AFM. More detailed studies which combine different methods should be performed to clarify these apparent differences.

The XRD data indicate that illitization occurs with a progressive increase in the proportion of illite-like layers. The absence of I3 sequences in the sample for which XRD indicates their presence, or the lack of any sequences which would be averaged by XRD to produce R3 ordering, implies that as the illite-like layer content of interstratified I-S increases, there is a tendency for illite-like layers to form together. That is, the TEM data imply that the range of R*n* I-S with large values of *n* does not normally include values of $n \geqslant 3$. Rather, a gap is implied to exist between I-S and illite. There is, however, complete agreement between both XRD and TEM data for R=1-rich samples, consistent with the implied relative stability of that material (*e.g.* Dong *et al.*, 1997). The collective data imply that (R=1) I-S is a relatively stable phase, and that it contains increasing proportions of I*n* (*n*>1) units with increasing grade; however, material for which some XRD data indicate the

https://doi.org/10.1346/000986002760832766 Published online by Cambridge University Press

presence of well-ordered I-S with R>1 have yet to be validated by direct observation of layer sequences by TEM.

Muscovite is the thermodynamically stable form of dioctahedral, aluminous micas, the precursor phases smectite, (R=1) I-S and illite being metastable, but relatively stable as compared with intermediate mixed-layered phases. That is, the Ponza Island samples are dominated by four discrete, ordered phases. These observations are in accord with several other recent TEM studies (*e.g.* Dong *et al.* , 1997; Yan *et al.*, 2001; Tillick *et al.*, 2001) in implying steps between discrete phases, including a gap in mixed-layering between (R=1) I-S and illite. The referenced studies also imply gaps between pure smectite and (R=1) I-S, but the samples chosen for TEM observations in this study unfortunately did not include one for which XRD data indicated the proportion of smectite in (R=0) I-S to be >0 and <50%.

Crystallization mechanism

Although many mechanisms have been proposed for illitization, two mechanisms represent the extremes: layer-by-layer replacement and bulk dissolution-crystallization. Altaner and Ylagan (1997) reviewed evidence for both mechanisms. They concluded that fluid/rock ratio and permeability influence reaction mechanisms, *e.g.* bentonites commonly have low permeabilities and resultant low fluid/rock ratios which inhibit large-scale dissolution and crystallization, whereas the high permeability of hydrothermal systems and sandstones promote dissolution and crystallization. They concluded that both dissolution/crystallization and solid-state transformation can occur in shales.

The BSE images of Ponza samples show irregularly-shaped cavities filled by the various dioctahedral clay minerals and the zeolite mordenite. These textures, combined with the euhedral shapes of some illitic phases and mordenite, provide direct evidence for neocrystallization from a fluid. That is supported by observations of euhedral shapes for I-S and illite as described by Ylagan *et al.* (1996). Such textures provide strong evidence for crystallization from cavity walls inward, via a fluid, following dissolution of precursor phases. The nature of the alteration process itself, *i.e.* hydrothermal alteration, implies such direct interaction of solids in a fluid-dominated environment.

Layer-by-layer replacement is commonly referred to as a solid-state transformation since reactants and products are in close, structurally-related contact, although Altaner and Ylagan (1997) note that small proportions of fluids may be present. If the solid-state transition mechanism operated, one expects to commonly observe along-layer transitions in TEM images, as has been observed in a plethora of studies involving replacement of one clay mineral by another (*e.g.* Ahn and Peacor, 1987; Banfield and Eggleton, 1988). Such transitions were not observed with certainty despite careful observations of many TEM images. The lack of direct evidence for layer-by-layer replacement in the present study does not indicate that this process may be rejected based only on TEM observations of layer sequences, but it is strong permissive evidence.

The collective data therefore imply that the clay minerals of Ponza Island formed via a dissolution-neocrystallization process. The dissolution-neocrystallization mechanism discussed by Altaner and Ylagan (1997) involves dissolution of precursor phyllosilicates, implying that a clay mineral such as illite was preceded by the sequence of I-S phases, starting with smectite. The TEM and SEM observations of this study produced no evidence of precursor phases; *e.g.* no reaction interfaces between smectite and a phase of greater reaction progress were observed. As noted above, no along-layer transitions were observed. There is therefore no evidence that a phase such as illite was preceded at its present site by a lower-grade clay mineral. Similar observations were made by Yan *et al.* (2001) and Tillick *et al.* (2001) for hydrothermally-altered silicic volcanic rocks. Their observations and those of this study suggest, but do not prove, that clay minerals in hydrothermal environments may form directly from fluids via neocrystallization following dissolution of original rock phases, such as volcanic glass. Such a mechanism has been postulated to have dominated the formation of phyllosilicates in the Salton Sea geothermal field, for example (Giorgetti, pers. comm.).

Mechanism for change in feldspar compositions

Ylagan *et al.* (1996) showed that much feldspar with compositions near end-members albite and K-feldspar are clearly authigenic in origin, some feldspar grains have the irregular shapes typical of detrital grains having been deposited as clastic material. Their angular, irregular shapes imply that they have not undergone significant dissolution. Their compositions are typical of the pure end-members, albite and microcline, with little or no solid-solution of Na and K. McDowell (1986) noted that alkali feldspars in shallow sediments of the Salton Sea Geothermal System (SSGF) had compositions typical of feldspars of volcanic origin, in that compositions spanned the range of the $KAlSi_3O_8$–$NaAlSi_3O_8$ binary system, but that compositions shifted toward those of the pure end-members with increasing depth. Giorgetti *et al.* (pers. comm.) observed in SSGF samples from the core drilled by the Salton Sea Scientific Drilling Program and concluded that even detrital feldspars in shallow sediments had end-member compositions. They concluded that Na and K compositions of feldspars must have changed through solid-state diffusion in crystals in contact with hydrothermal fluids, but at temperatures $<<100^{\circ}C$. Similarly, the end-member compositions which are atypical of quenched volcanic grains, combined with unaltered grain shapes of

feldspars in the present study likewise imply that they have changed composition via solid-state diffusion. Such a mechanism is well-known to experimentalists, but at much higher temperatures. The observations of this study, however, imply that it is a significant process during diagenesis at temperatures corresponding to formation of I-S. Such exchange of Na and K between feldspars and pore-fluids must therefore be a significant factor in determining the Na and K content of pore-fluids, which in turn mediate the formation of illite. The K-feldspar which was so-formed may serve as a source of K during illitization, as defined in the classic relations of Hower *et al.* (1976).

Relation between mordenite and illitization

The smectite which was observed to have altered directly from volcanic glass has Na as the dominant interlayer cation, as does the glass. As Masuda *et al.* (1996) showed where such smectite is K-rich, the composition of smectite reflects that of the altering glass, implying that the interlayer cation results from local interplay at the reaction interface, rather than as buffered by fluid composition. Although the precise timing of the formation of I-S and mordenite cannot be determined based on the observations of this study, the association of neoformed, euhedral mordenite with I-S is clearly defined. Sodium is the dominant alkali or alkaline earth element in mordenite. We suggest that the parallelism of formation of mordenite concomitant with crystallization of I-S with increasing proportions of K-rich illite-like layers is a result of the availability of Na in pore-fluids made possible by the decreasing proportion of smectite-like layers. That such interrelationships are possible was demonstrated by Masuda *et al.* (1996). They showed, in bentonites of the Nankai Trench, that the interlayer cations in smectite coexisting with various zeolites change as new zeolites form which are dominated by other cations, *i.e.* formation of a Na-rich zeolite was paralleled by a decrease in the proportion of Na in smectite interlayers.

Polytypic changes

Ylagan's results (Ylagan, 1996; Ylagan *et al.*, 1996) indicate that dioctahedral clays change progressively from *cis*-vacant, turbostratically-stacked smectite, to interstratified *cis*- and *trans*-vacant, $1M_d$ I-S, to *trans*-vacant, $1M$ illite, and then to $2M_1$ illite in Ponza Island samples. The SAED patterns of I-S and illitic phases from samples 93-6-9Q, 93-6-8N, and 93-6-10A indicate the predominance of $1M_d$ polytypism both in I-S and illitic phases, and the coexistence in the more altered samples of $1M_d$ illite and 2-layer polytypes of mica, implied to be $2M_1$ as is normally the case. The TEM data show only $1M_d$ and $2M_1$ polytypism, however, without the intermediate $1M$ polytype generally assumed to exist in prograde sequences, as first implied by Yoder and Eugster (1955), and later observed using powder XRD of natural sediments (*e.g.* Velde and Hower, 1963; Maxwell and Hower, 1967; Lee *et al.*, 1985). However, several TEM studies of prograde sequences from different geological environments failed to find the supposed intermediate polytype $1M$, instead reporting only a transition from $1M_d$ to $2M_1$ (*e.g.* Grubb *et al.*, 1991; Dong and Peacor, 1996; Bauluz *et al.*, 2000). The $1M$ polytype was definitively observed in only a few instances including in the Potsdam Sandstone, Silverton Caldera, Broadlands-Ohaaki geothermal field, and Golden Cross gold mine, generally coexisting with $2M_1$ illite or mica, as recently confirmed in all cases by TEM (Dong, pers. comm.). The data of Zoeller and Brockamp (1997) for coexisting $2M_1$ and $1M$ material imply that the latter is relatively rich in Mg and Fe and this has been confirmed by (Dong, pers. comm.) for the $1M$ occurrences listed above, suggesting that the occurrence of the $1M$ polytype in prograde systems could be a function of the Fe and Mg availability in those environments.

The presence of non-00l reflections with $k \neq 3N$, which are ill-defined, non-periodic and diffuse parallel to $\mathbf{c}^*$ in SAED patterns of the I-S and illitic phases described above, implies that stacking is random but with local coherency. Such reflections are better defined with increasing degree of illitization, implying an increase in proportion of coherently or semi-coherently related layers. Although the smaller effective wavelength of TEM permits sensing of smaller ordered units than for XRD, such stacking order must have an expression in XRD patterns. We tentatively suggest that such effects, as an average over a complex array of locally ordered and disordered stacking units, must be detectable on XRD patterns. We can not predict the exact effect, but because Ylagan *et al.* (2000) observed $1M$ polytypism in a sample for which TEM shows no such relation, the effect may be interpreted as being due to the presence of a well-ordered $1M$ polytype where none exists. Dong and Peacor (1996) used cross fringes in TEM images to show that stacking sequences giving SAED patterns indicating $1M_d$ polytypism tended to be of the $2M_1$-type, even though such order did not occur over layer sequences large enough to show well-ordered $2M_1$ polytypism. They interpreted this to be a precursor to $2M_1$ mica which might form at higher grades. Similarly, Tillick *et al.* (2001), in Golden Cross gold-mine samples, observed weak, local $1M$ order in I-S which was a precursor to well-ordered $1M$ illite at higher grades. The material identified as $1M_d$ by TEM may therefore have a tendency to $1M$ stacking where there is local coherent stacking, but not sufficient to be detected in SAED patterns. Perhaps the average of coherently stacked units may be sensed as $1M$ by XRD, however.

Possible evidence for octahedral cation distributions in SAED patterns

Although SAED patterns corresponding to the $1M_d$ polytype from the Ponza Island samples are superficially

similar, there are regular differences in the relative intensities of the 00*l* reflections. The basal reflections observed in the SAED patterns of sample 93-6-8C (smectite) are progressively less intense with increasing order; those of samples 93-6-9Q and 93-6-8N (R=1 and highly illitic I-S) have $I_{001} > I_{003} > I_{002}$, whereas those of sample 93-6-10A (illite) have $I_{003} > I_{001} > I_{002}$.

On the other hand, we observed a clear correlation between the chemical compositions as determined by AEM, reported in this study, and P*cv* as determined by Ylagan (1996) and Ylagan *et al.* (2000). A decrease in P*cv* values correlates with increase in K [*r* (correlation coefficient) = 0.98], Al(tot) (*r* = 0.96), and Fe+Mg (*r* = 0.98) contents. The distribution of octahedral cations within octahedral sheets therefore changes in the studied samples with increasing degree of illitization, as concluded by Drits (1987) and McCarty and Reynolds (1998) in other samples. We suggest that the differences in intensities of 00*l* reflections may be a function of such differences, and that observation of 00*l* intensities of SAED patterns may therefore be used as a qualitative measure of divalent cation proportions in octahedral sheets. On the other hand, the relation between the chemical composition of the octahedral sheet, the P*cv* values and the 00*l* intensities of SAED patterns suggest that more studies are needed to determine if the proportion of *cis*- or *trans*-vacant sites (P*cv* values) can be inferred directly from the 00*l* intensities of SAED patterns.

CONCLUSIONS

Dioctahedral phyllosilicates in altered rhyolitic hyaloclastite from Ponza (Italy) pseudomorph lapilli fragments, preserve vesicular textures and, therefore, samples retain original texture. The lowest-grade sample contains obsidian clasts partially replaced by smectite, and the proportion of illite increases as alteration grade increases, with the occurrence of interstratified I-S, zeolites, illitic phases, feldspars and quartz. The most altered sample contains illite, mica and quartz.

Textural studies, by SEM and TEM, show that subhedral dioctahedral clay minerals and mordenite fill irregular cavities, providing direct evidence for neocrystallization from a fluid. The presence of discrete phases without features such as along-layer transitions at the TEM scale further implies that all clay minerals may have formed simultaneously by direct crystallization from fluids. This mechanism occurs without prior crystallization of, or transformations from, lower-grade I-S, and reaction progress may be determined by variations in temperature and/or rock/fluid ratio.

The TEM data show that the sequence proceeds through smectite, $1M_d$ (R=1) I-S, $1M_d$ highly illitic I-S, and $1M_d$ illite plus $2M_1$ mica. The (R=1) I-S is the only ordered I-S phase detected, with a lack of interstratification between (R=1) I-S and illite implying a gap in mixed-layering between these two phases. The described illitization process is accompanied by an increase in K, total Al content, and Fe plus Mg content in the octahedral sheet of the dioctahedral phyllosilicates; systematic changes in the basal reflection intensities of SAED patterns of these phases probably reflect the octahedral sheet composition variations. The 1*M* polytype does not occur, in contrast with XRD data.

ACKNOWLEDGMENTS

The authors thank G. Guthrie and an anonymous reviewer for helpful suggestions for improving the manuscript. B. Bauluz is grateful to C.E. Henderson and L.-S. Kao for technical assistance at the University of Michigan and to Y. Yan for help in sample preparation. This work was supported by National Science Foundation grants EAR 9418108 and 9814391 to D.R. Peacor.

REFERENCES

Ahn, J.H. and Peacor, D.R. (1986) Transmission and analytical electron microscopy of the smectite-to-illite transition. *Clays and Clay Minerals*, **34**, 165–179.

Ahn, J.H. and Peacor, D. R. (1987) Kaolinitization of biotite: TEM data and implications for an alteration mechanism. *American Mineralogist*, **72**, 353–356.

Ahn, J.H. and Peacor, D.R. (1989) Illite/smectite from Gulf Coast shales: a reappraisal of transmission microscope images. *Clays and Clay Minerals*, **37**, 542–546.

Altaner, S.P., Whitney, G., Aronson, J.L. and Hower, J. (1984) A model for K-bentonite formation, evidence from zoned K-bentonites in the disturbed belt, Montana. *Geology*, **12**, 412–415.

Altaner, S.P., Weiss, C.A. Jr. and Kirkpatrick, R.J. (1988) Evidence from ^{29}Si NMR for the structure of mixed-layer illite/smectite clay minerals. *Nature*, **331**, 699–702

Altaner, S.P. and Ylagan, R.F. (1997) Comparison of structural models of mixed-layer illite/smectite and reaction mechanisms of smectite illitization. *Clays and Clay Minerals*, **45**, 517–533.

Banfield, J.F. and Eggleton, R.A. (1988) Transmission electron microscope study of biotite weathering. *Clays and Clay Minerals*, **36**, 47–60.

Barbieri, F., Borsi, S., Ferrara, G. and Innocenti, F. (1967) Contributo alla conoscenza vulcanologica e magmatologica elle isole dell'arcipelago Pontino. *Memoria della Societa Geologica Italiana*, **17**, 581–606.

Barron, P.F., Slade, P. and Frost, R.L. (1985) Ordering of aluminum in tetrahedral sites in mixed-layer 2:1 phyllosilicates by solid-state high-resolution NMR. *Journal of Physical Chemistry*, **89**, 3880–3885.

Bauluz, B., Peacor, D. and Gonzalez Lopez, J.M. (2000) Transmission Electron Microscopy study of illitization in pelites from the Iberian Range, Spain: layer-by-layer replacement? *Clays and Clay Minerals*, **48**, 374–384.

Brusewitz, A. (1986) Chemical and physical properties of Paleozoic potassium bentonites from Kinnekulle, Sweden. *Clays and Clay Minerals*, **34**, 442–454.

Carmassi, M., De Rita, D., Di Filippo, M. and Funiciello, R. (1983) Geology and volcanic evolution of the island of Ponza, Italy. *Geologica Roma*, **22**, 211–232.

Dong, H. and Peacor, D.R. (1996) TEM observations of coherent stacking relations in smectite, I/S and illite of shales: evidence for MacEwan crystallites and dominance of $2M_1$ polytypism. *Clays and Clay Minerals*, **44**, 257–275.

Dong, H., Peacor, D.R. and Freed, R.L. (1997) Phase relations

among smectite, R1 illite-smectite and illite. *American Mineralogist*, **82**, 379–391.

Drits, V.A. (1987) Mixed-layer minerals: Diffraction methods and structural features. Pp. 33–45 in: *Proceedings of the International Clay Conference, Denver, 1985* (L.G. Schultz, H. Van Olphen and F.A. Mumpton, editors). The Clay Minerals Society, Bloomington, Indiana.

Grim, R.E. and Güven, N. (1978) *Bentonites: Geology, Mineralogy, Properties and Uses*. Elsevier, Amsterdam, The Netherlands.

Grubb, S.M.B., Peacor, D.R. and Jiang W.-T. (1991) Transmission electron microscope observations of illite polytypism. *Clays and Clay Minerals*, **39**, 540–550.

Guthrie, G.D. and Veblen, D.R. (1989a) High-resolution transmission electron microscopy of mixed-layer illite/smectite: Computer simulation. *Clays and Clay Minerals*, **37**, 1–11.

Guthrie, G.D. and Veblen, D.R. (1989b) High-resolution transmission electron microscopy applied to clay minerals. In *Spectroscopic Characterization of Minerals and their Surfaces* (L.M. Coyne, S.W.S. McKeever and D.F. Blake, editors). Symposia Series 415, American Chemical Society, Washington, D.C.

Guthrie, G.D. and Veblen, D.R. (1990) Interpreting one-dimensional high-resolution transmission electron micrographs of sheet silicates by computer simulation. *American Mineralogist*, **75**, 276–288.

Güven, N. and Grim, R. (1972) X-ray diffraction and electron optical studies on smectite and α-cristobalite associations. *Clays and Clay Minerals*, **20**, 89–92.

Horton, D.G. (1985) Mixed-layer illite/smectite as a paleotemperature indicator in the Amethyst vein system, Creed district, Colorado, USA. *Contributions to Mineralogy and Petrology*, **91**, 171–179.

Hower, J., Eslinger, E.V., Hower, M.E. and Perry, E.A. (1976) Mechanism of burial metamorphism of argillaceous sediments: Mineralogical and chemical evidence. *Geological Society of America Bulletin*, **87**, 725–737.

Jadgozinski, H. (1949) Eindimensionale fehlordnung in kristallen und ihr einfluss auf die Rontgeninterferenzen. I. Berechnung des fehlordnungsgrades au der Rontgenintensitaten. *Acta Crystallographica*, **2**, 201–207.

Jakobsen, H.J., Nielsen, N.C. and Lindgreen, H. (1995) Sequences of charged sheets in rectorite. *American Mineralogist*, **80**, 247–252.

Jiang, W.-T., Peacor, D.R., Merriman, R.J. and Roberts, B. (1990) Transmission and analytical electron microscopic study of mixed-layer illite/smectite formed as an apparent replacement of product of diagenetic illite. *Clays and Clay Minerals*, **38**, 449–469.

Jiang, W.-T. and Peacor, D.R. (1993) Formation and modification of metastable intermediate sodium potassium mica, paragonite and muscovite in hydrothermally altered metabasites from northern Wales. *American Mineralogist*, **78**, 782–793.

Kim, J.W., Peacor, D.R., Tessier, D. and Elsass, F. (1995) A technique for maintaining texture and permanent expansion of smectite interlayers for TEM observations. *Clays and Clay Minerals*, **43**, 51–57.

Lee, J.H.K., Peacor, D.R., Lewis, D.D. and Wintsch, R.P. (1985) Chlorite-illite/muscovite interlayered and interstratified crystals: A TEM/STEM study. *Contributions to Mineralogy and Petrology*, **88**, 372–385.

Lombardi, G. and Mattias, P. (1981) *Guidebook for the Excursions in Sardinia and Central Italy*. AIPEA, Rome, 96 p.

Lupino, R. (1954) Sulla bentonite dell'isola di Ponza. *La Ricerca Scientifica*, **24**, 2326–2339.

McCarty, D. and Reynolds, R.C. Jr. (1998) Rotationally disordered illite/smectite in Paleozoic K-bentonites. *Clays and Clay Minerals*, **43**, 271–284.

Malinverno, A. and Ryan, W.B.F. (1986) Extension in the Tyrrenian Sea and shortening in the Apennines as a results of arc migration driven by sinking of the lithosphere. *Tectonophysics*, **5**, 228–245.

Masuda, H., O'Neil, J., Jiang, W.-T. and Peacor, D. (1996) Relation between interlayer composition of authigenic smectite, mineral assemblages, I/S reaction rate and fluid composition in silicic ash of the Nankai Trough. *Clays and Clay Minerals*, **44**, 443–459.

Masuda, H., Peacor, D.R. and Dong, H. (2001) TEM study of conversion of smectite to illite in mudstones of the Nankai Trough: Contrast with coeval bentonites. *Clays and Clay Minerals,* **49**, 109–118.

Maxwell, D.T. and Hower, J. (1967) High-grade diagenesis and low-grade metamorphism of illite in the precambrian belts series. *American Mineralogist*, **52**, 843–857.

McDowell, S.D. (1986) Composition and structural state of coexisting feldspars, Salton Sea geothermal field. *Mineralogical Magazine*, **50**,75–84.

Nadeau, P.H., Wilson, M.J., McHardy, W.J. and Tait, J.M. (1985) The conversion of smectite to illite during diagenesis. Evidence from some illitic clays from bentonites and sandstones. *Mineralogical Magazine*, **49**, 393–400.

Passaglia, E., Artioli, G. Gualtieri, A. and Carnevali, R. (1995) Diagenetic mordenite from Ponza Italy. *European Journal of Mineralogy*, **7**, 429–438.

Peccerilli, A. (1985) Roman comagmatic province (Central Italy): Evidence for subduction-related magma genesis. *Geology*, **13**, 103–106.

Pichler, H. (1965) Acid Hyaloclastites. *Bulletin of Volcanology*, **28**, 293–312.

Pozzuoli, A. (1988) Mineralogy, geochemistry, and origin of alteration products in the Pontina archipelago, Italy. 1. The genesis of the Ponza bentonite. Pp. 89–98 in: *Proceedings of the 10th Conference on Clay Mineralogy and Petrology* (J. Konta, editor). Ostrava, Czechoslovakia.

Savelli, C. (1983) Eta'K/Ar delle principali manifestazioni riolitiche dell'isola di Ponza. *Rendiconti Societa Geologica Italiana*, **6**, 39–42.

Savelli, C. (1987) K/Ar ages and chemical data of volcanism in the western Pontine Islands (Tyrrhenian Sea). *Bolletino Societa Geologica Italiana*, **106**, 537–546.

Tillick, D.A., Peacor, D.R. and Mauk, J.L. (2001) Genesis of dioctahedral phyllosilicates during hydrothermal alteration of volcanic rocks: I. The Golden Cross epithermal ore deposit, New Zealand. *Clays and Clay Minerals*, **49**, 126–140.

Veblen, D.R., Guthrie, G.D. Jr., Livi, K.J.T. and Reynolds, R.C. Jr. (1990) High-resolution transmission electron microscopy and electron diffraction of mixed-layer illite/smectite: Experimental results. *Clays and Clays Minerals*, **38**, 1–13.

Velde, B. and Hower, J. (1963) Petrological significance of illite polymorphism in sedimentary rocks. *American Mineralogist*, **48**, 1239–1254.

Yan, Y., Tillick, D.A., Peacor, D.R. and Simmons, S.F. (2001) Genesis of dioctahedral phyllosilicates during hydrothermal alteration of volcanic rocks: The Broadlands hydrothermal system, New Zealand. *Clays and Clay Minerals*, **49**, 141–155.

Ylagan, R.F. (1996) Mineralogy and geochemistry associated with hydrothermal alteration of a rhyolitic hyaloclastite from Ponza Island, Italy. PhD thesis. University of Illinois, USA, P. 152.

Ylagan, R.F., Altaner, S., Pozzuoli, A. (1996) Hydrothermal alteration of a rhyolitic hyaloclastite from Ponza Island, Italy. *Journal of Volcanology and Geothermal Research*, **74**, 215–231.

Ylagan, R.F., Altaner, S.P. and Pozzuoli, A. (2000) Reaction Mechanisms of Smectite Illitization associated with hydrothermal alteration from Ponza Island, Italy. *Clays and Clay Minerals*, **48**, 610–631.

Yoder, H.S. and Eugster, H.P. (1955) Synthetic and natural muscovites. *Geochimica et Cosmochimica Acta*, **8**, 225–280.

Zoeller, M. and Brockamp, O. (1997) 1M- and $2M_1$-illites: different minerals and not polytypes. Results from single crystal investigations at the Transmission Electron microscope (TEM). *European Journal of Mineralogy*, **9**, 821–827.

(*Received 3 January 2001; revised 14 June 2001; Ms. 508*)